Lawrence Berkeley National Laboratory
Lawrence Berkeley National Laboratory

Title
REVIEW OF NEW RESULTS ON MULTILEPTON PRODUCTION BY MUONS

Permalink
https://escholarship.org/uc/item/6qs0j2vh

Author
Strovink, Mark

Publication Date
1980-05-01

eScholarship.org Powered by the California Digital Library
University of California

LBL-10989 C. II

Lawrence Berkeley Laboratory
UNIVERSITY OF CALIFORNIA

Physics, Computer Science & Mathematics Division

Invited paper presented at the XVth Rencontre de Moriond, Les Arcs, Savoie, France, March 9-21, 1980

REVIEW OF NEW RESULTS ON MULTILEPTON PRODUCTION BY MUONS

Mark Strovink

May 1980

RECEIVED
LAWRENCE
BERKELEY LABORATORY
AUG 01 1980
LIBRARY AND
DOCUMENTS SECTION

TWO-WEEK LOAN COPY

This is a Library Circulating Copy which may be borrowed for two weeks. For a personal retention copy, call Tech. Info. Division, Ext. 6782.

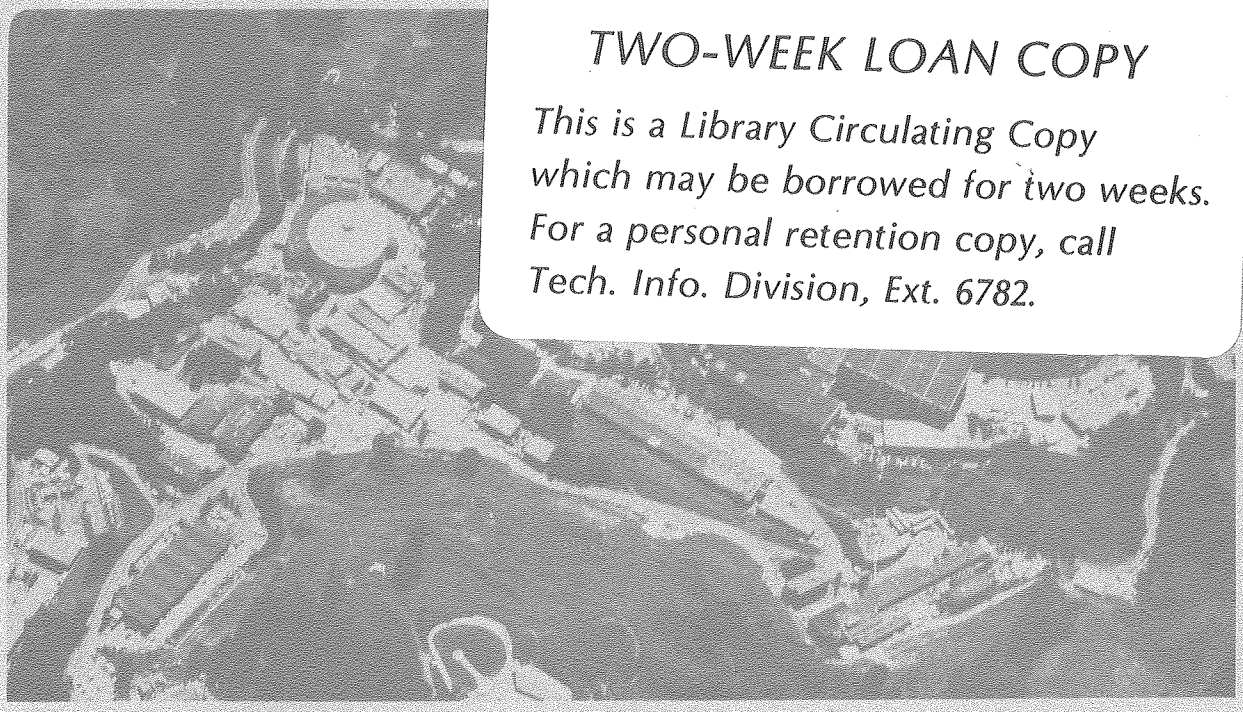

Prepared for the U.S. Department of Energy under Contract W-7405-ENG-48

LBL 10989 C.II

DISCLAIMER

This document was prepared as an account of work sponsored by the United States Government. While this document is believed to contain correct information, neither the United States Government nor any agency thereof, nor the Regents of the University of California, nor any of their employees, makes any warranty, express or implied, or assumes any legal responsibility for the accuracy, completeness, or usefulness of any information, apparatus, product, or process disclosed, or represents that its use would not infringe privately owned rights. Reference herein to any specific commercial product, process, or service by its trade name, trademark, manufacturer, or otherwise, does not necessarily constitute or imply its endorsement, recommendation, or favoring by the United States Government or any agency thereof, or the Regents of the University of California. The views and opinions of authors expressed herein do not necessarily state or reflect those of the United States Government or any agency thereof or the Regents of the University of California.

LBL-10989

REVIEW OF NEW RESULTS ON MULTILEPTON PRODUCTION BY MUONS

Mark Strovink

Physics Department and Lawrence Berkeley Laboratory,
University of California, Berkeley, California 94720

Invited Paper presented at the
XVth Rencontre de Moriond
Les Arcs - Savoie - France
March 9-21, 1980

ABSTRACT

New multimuon data primarily from the Berkeley-Fermilab-Princeton and European Muon Collaborations are reviewed. Relative to elastic muoproduction of $J/\psi(3100)$, ψ events produced at finite but low inelasticity are distributed steeper in ν and Q^2 and flatter in $-t$. The transverse polarization of elastically produced ψ final states is oriented as expected from s-channel helicity conservation, but gives way to substantial longitudinal polarization at $Q^2 \gtrsim 2(\mathrm{GeV/c})^2$. At 209 GeV, the diffractive open-charm muoproduction cross section is $6.9^{+1.9}_{-1.4}$ nb, and the $Q^2 \to 0$ photon cross sections are 750^{+180}_{-130} (560^{+200}_{-120}) nb at 178(100) GeV. The ψ data and open-charm data both with single and double charm decay to muons generally confirm the photon-gluon-fusion model predictions. Diffractive charm production accounts for $\sim 1/3$ of the scale-noninvariance observed in muon-nucleon scattering at low Bjorken x.

RESUMÉ

Je présente de nouvelles données, provenant essentiellement des groupes Berkeley-Fermilab-Princeton et European Muon Collaboration, sur la production par des muons d'évènements à plusieurs muons. Comparée à celle de la production élastique du J/ψ, la distribution des ψ produits a inélasticité faible mais finie apparait plus pentue en ν et Q^2 et plus plate en $-t$. La polarisation transverse des ψ élastiques est orientée comme on l'attend de la conservation de l'hélicité en voie s, mais laisse place à une substantielle polarisation longitudinale à $Q^2 > 2$ $(\mathrm{GeV/c})^2$. A 209 GeV la section efficace de production diffractive du charme apparent par des muons est $6.9^{+1.9}_{-1.4}$ nb et les sections efficaces pour des photons à la limite $Q^2 = 0$ sont respectivement 750^{+180}_{-130} et 560^{+200}_{-120} nb à 178 et 100 GeV. Les données sur le ψ et le charme apparent tant lorsque la désintégration en muons du charme est simple que double confirme en général les prédictions du modèle de fusion photon-gluon. La production diffractive de charme rend compte d'un tiers de la violation de l'invariance d'echelle observée dans la diffusion muon-nucleon à faible x de Bjorken.

I. INTRODUCTION

This Rencontre marks the first opportunity to review extensive data on the virtual photoproduction of charmed-quark pairs, both bound and unbound. I shall emphasize new results from the Berkeley-Fermilab-Princeton (BFP) collaboration[1] and the European Muon Collaboration[2] (EMC) on $J/\psi(3100)$ and $c\bar{c}$ muoproduction, with subsequent muonic decay. Results from the Bologna-CERN-Dubna-Munich-Saclay (BCDMS) and Michigan State-Fermilab (MSUF) muon experiments are also important to mention.

Section II is devoted to heavy-quarkonium muoproduction. After briefly reviewing the BCDMS limit[3] on Υ muoproduction and the published data[4,5] on elastic ψ muoproduction, I shall concentrate on new results in two areas: inelastic ψ muoproduction (EMC), and polarization of elastically produced ψ's (BFP). Section III, the bulk of this review, presents first results on open-charm muoproduction from the BFP and EMC groups. The EMC results include early observations of double charm decay to muons; the BFP data[6,7] represent a 40-fold increase in statistics over the MSUF single-charm-decay sample[8]. I shall conclude with a quantitative determination[7] of the contribution of charm production to scale-noninvariance in inclusive deep-inelastic muon-nucleon scattering.

The theoretical framework for discussion of charm leptoproduction is evolving rapidly. In 1976 Sivers, Townsend and West[9] obtained a lower bound on the total ψN cross-section, requiring measurement of the ratio of cross-sections for forward ψ and total charm photoproduction. This bound depends only on unitarity and OZI[10] rules. Adding traditional vector-meson dominance (VMD) assumptions makes the ratio of elastic to total ψN cross-sections nearly equal to the ratio of elastic ψ to total charm photoproduction. This ratio is evaluated in Ref. 9 as $(0.013\pm0.004)/\lambda$, where $\lambda\approx0.7$ is an off-shell correction. VMD connects charm photoproduction to charm muoproduction via a $(1+Q^2/m_\psi^2)^{-2}$ ψ propagator. The original data[8] on open-charm muoproduction were analyzed using a phenomenological "photon dissociation" model of Bletzacker and Nieh (BN)[11].

With the advent of quantum chromodynamics, recent activity has centered on the photon-gluon-fusion (γGF) model[12], to which the graph below and at right re-

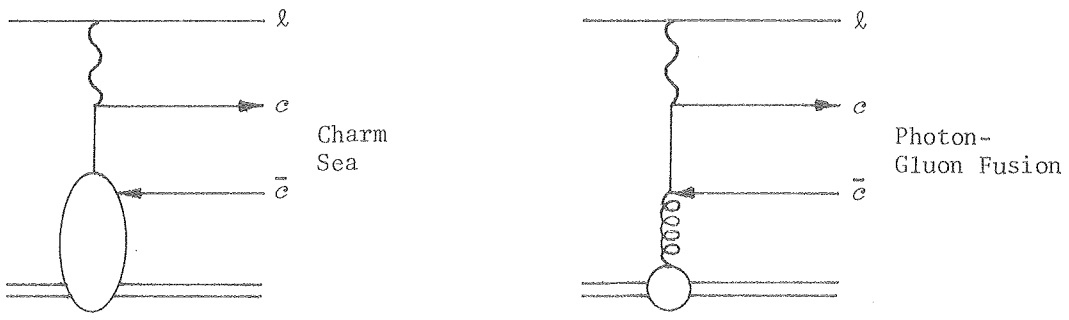

fers. This is a Bethe-Heitler diagram for charmed-quark pair production with the nuclear photon replaced by a gluon. Not shown are the additional (presumably) soft gluon exchanges needed to conserve color. Comparison with the graph at left emphasizes the close connection between photon-gluon-fusion and the charmed sea. The large mass m_c associated with the internal quark line makes the gluon-exchange diagram finite and possibly the leading contributor to the charmed sea. Specific use of that mechanism makes it possible to allow sensibly for threshold effects due to m_c, and to predict the experimentally important correlation between the momenta of the two charmed quarks. In particular, the γGF model unifies the description of closed and open charm production via the quark pair mass $m_{c\bar{c}}$: charmonium production is taken to be dual to $c\bar{c}$ production with $2m_c<m_{c\bar{c}}<2m_D$, while open-charm production has $m_{c\bar{c}}>2m_D$. This makes the γGF charmonium calculations much more sensitive to m_c than are the open-charm calculations. Typically, one assumes $m_c=1.5$ GeV/c^2 and $\alpha_s=1.5/\ell n(m^2_{c\bar{c}}/\Lambda^2)$ with $\Lambda=0.5$ GeV/c^2. The distribution in gluon momentum fraction x is usually taken to be $3(1-x)^5/x$, with the exponent set by counting-rule arguments[13] and the coefficient by the integral over Bjorken $x_B=Q^2/2m_p\nu$ of the measured inelastic structure function $F_2(x_B,Q^2)$. The fraction of charmonia realized as the ψ is perhaps best regarded as a fit parameter[14] with the value 1/6. With these choices, at 209 GeV the total cross section for (presumably primarily elastic) ψ muoproduction is 0.47 nb, and for open $c\bar{c}$ muoproduction is 5.0 nb. A similar calculation with bottom quarks of mass 4.7 GeV/c^2 and charge 1/3 gives 0.28 pb for Υ muoproduction at 275 GeV.

II. QUARKONIUM MUOPRODUCTION

In advance of the detailed discussion of charmonium production, I shall mention the BCDMS limit on Υ muoproduction reported[3] at the 1979 Lepton-Photon Symposium. Their 90% confidence limit is $\sigma(\mu N\to\Upsilon X)B(\Upsilon\to\mu^+\mu^-)<(6\pm3)\times10^{-39}$ cm^2 at ∿275 GeV, where the error is systematic. With $B(\Upsilon\to\mu^+\mu^-)=(3.1\pm0.9)\%$[15], the above γGF calculation predicts $\sigma B=(8.7\pm2.5)\times10^{-39}$ cm^2, almost violating the BCDMS bound. Their reported effective integrated luminosity is $(\varepsilon_\Upsilon=0.48)\times(N_\mu=1.5\times10^{11})\times(10\times500\times1.55\times6\times10^{23})=0.33\times10^{39}$ cm^{-2}. Therefore, the BCDMS limit corresponds to ≤2 Υ candidates (90% confidence). In fact, the experiment observed 24 events between 8 and 12 GeV/c^2 in dimuon mass, over a calculated background of 30 electromagnetic tridents. Presumably, if the background estimate were reduced by a factor of 2, the limit would weaken by a larger factor.

Some of the published results[4,5] from BFP and EMC on elastic ψ muoproduction are summarized in Table I. The original comparison[4] of the measured ν-dependence with the available γGF prediction[16] found serious disagreement. Weiler[17] and Barger, Keung and Phillips[14] have repeated the calculation and obtained much better agreement with the data. Using a $(1-x)^n/x$ gluon distribu-

TABLE I. Comparison of elastic and inelastic ψ muoproduction data.

$\sigma_{eff}(\gamma_V N \to \psi X)$	Elastic (BFP) (Ref. 4)	Elastic (EMC) (Ref. 5)	Inelastic (EMC)
ν-dependence	~log $\nu/10$ consistent with γ-G fusion		~exp $(\nu/55)$
Q^2-dependence: $(1+Q^2/\Lambda^2)^{-2}$, Λ=	2.7±0.5	2.4±0.3	1.8±0.2
$-t$ slope: $\exp(bt)$, b=	2 components $\langle b\rangle$ ~ 2.4	2.3±0.3	~1
Dependence on $z=E_\psi/\nu$	$\equiv\delta(z-1)$		~z^2, $z\gtrsim 0.5$

tion, they fit $n=5.6^{+0.8}_{-1.2}$, and $n=4.6$, respectively. A diffractive behavior $\exp(bt)$ in momentum-transfer-squared $-t$ to hadrons is observed, with $b\approx 2$-3 $(\mathrm{GeV/c})^{-2}$ as in ψ photoproduction[18]. The measured Q^2-dependence is fit by a propagator $(1+Q^2/\Lambda^2)^{-2}$ with $\Lambda\approx 2.5$ GeV/c^2. That Λ is smaller than m_ψ is not yet firmly established. In any event, I argue in the latter part of this section that the observed Q^2-dependence of the polarization of produced ψ's immensely complicates the interpretation of these Q^2 fits.

Figure 1(a,b) shows EMC dimuon mass plots for (a) all events (304 ψ's), and (b) inelastic events (150 ψ's). The mass resolution at the ψ is 7% rms. Events

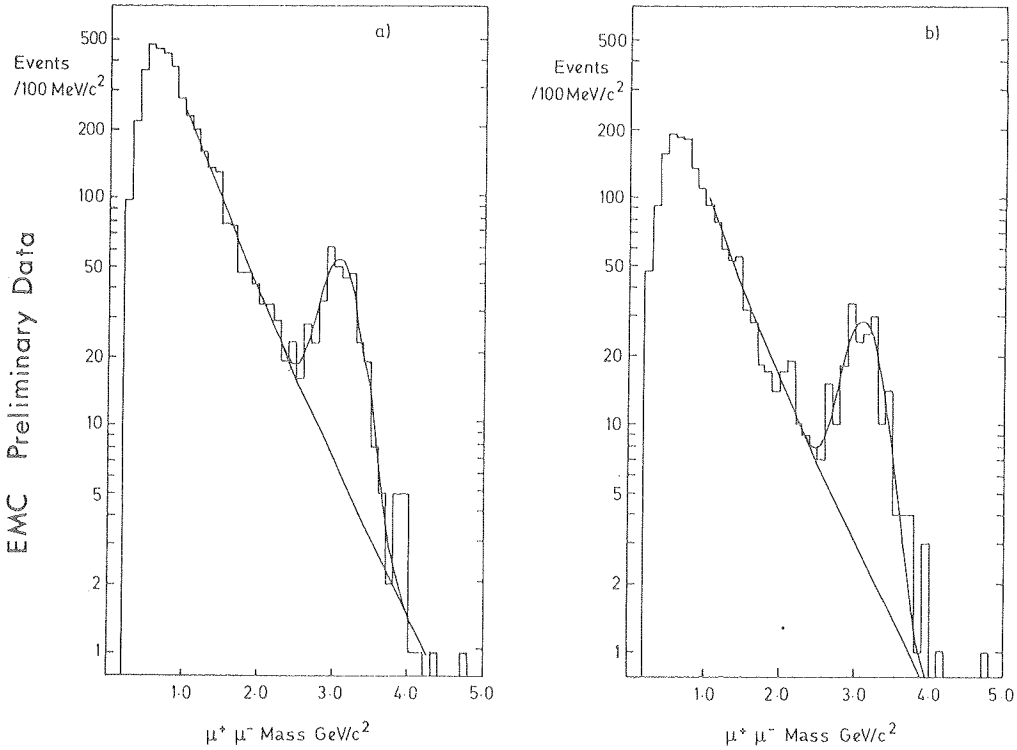

FIG. 1. Spectra of dimuon masses in EMC data at 280 GeV: (a) all data (304±22 ψ's); (b) inelastic data with $\geq$ 5 GeV calorimeter energy (150 ψ's). Included are data in which the third (scattered) muon is not momentum-analyzed.

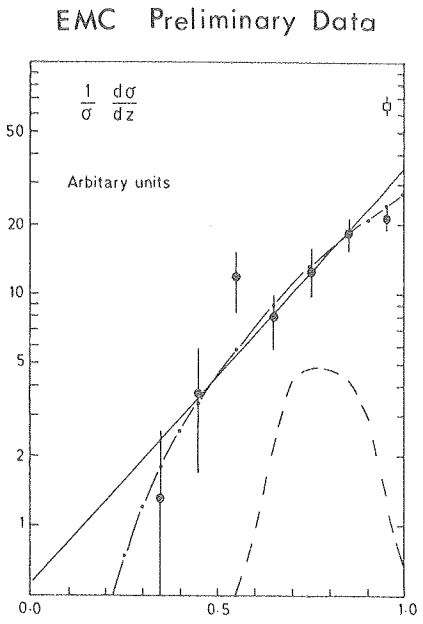

FIG. 2. Distribution in elasticity $z=E_\psi/\nu$ for ψ events with calorimeter energy >5 GeV (closed circles), and <5 GeV (open square, for clarity drawn at $z<1$). The solid and dot-dashed curves are proportional to $\exp(4z)$ and z^2, respectively. The dashed curve is a calculation for ψ' production with hadronic decay into ψ.

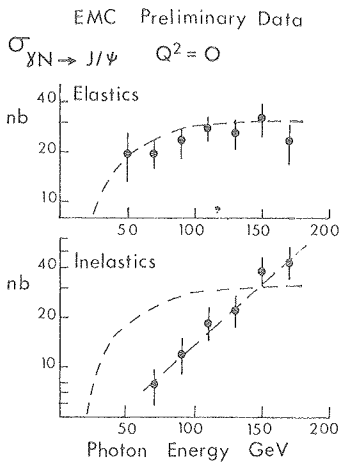

FIG. 3. Energy-dependence of the effective photon cross section for ψ production with calorimeter energy (top) <5 GeV, and (bottom) >5 GeV. Dashed curves are the elastic photon-gluon fusion prediction; the dashed line is $\propto \exp(\nu/55)$.

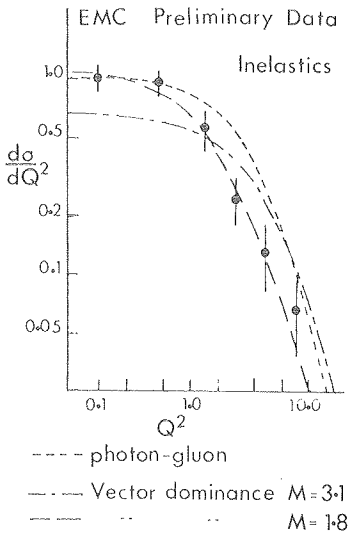

FIG. 4. Q^2-dependence of the effective photon cross section for ψ production with calorimeter energy >5 GeV. The dot-dashed (dashed) curves are $(1+Q^2/M^2)^{-2}$ with M set to 3.1 (fit to 1.8) GeV/c^2. The solid curve is the elastic photon-gluon-fusion prediction.

are defined to be inelastic if energy exceeding 5 GeV is deposited in the calorimeter near the vertex. Radiative corrections to elastic events explain ≈20 of the inelastic events. Figure 2 shows the $z=E_\psi/\nu$ distribution of the inelastic data, which are concentrated at high z. As indicated by the dashed curve, this is the region which would be populated by production and decay to ψ's of more massive charmonia, e.g. $\psi'\to\psi\pi\pi$. The estimated ψ' contribution is $\sim$1/3 of the rate observed at $z\approx0.75$. While consistent with ψ' photoproduction rates observed at SLAC[18], this estimate is not based on direct ψ' muoproduction measurements at SPS energies, which do not yet exist. Data above $z\approx0.9$ are very difficult to interpret; many radiative processes including production and decay to ψ's of $J\neq1$ charmonia can provide the small amount of calorimeter energy. All the data lie above the central rapidity region corresponding to $\langle z\rangle\approx0.2$, for which Leveille and Weiler[19] have made predictions.

Averaging over the z region and over the various contributing processes, the inelastic data are seen in Fig. 3(b) to possess a much steeper ν-dependence than do the elastic data (Fig. 3a). Both dashed curves in Fig. 3 are the same γGF

prediction for elastic ψ production. The inelastic ψ's have a smaller diffractive slope b and a steeper Q^2-dependence than do the elastic ψ's (Fig. 4). Table I summarizes the elastic/inelastic comparison. Beyond this first step, additional inelastic ψ data are needed in the region $z \lesssim 0.65$, which is essentially free of background from elastic production of excited charmonia.

The polarization of produced ψ's is readily analyzed by $\mu^+\mu^-$ decays. As in ψ hadroproduction, its study is expected to illuminate the production mechanism. In particular, if [for example, via s-channel helicity conservation[20] (SCHC)] the ψ helicity follows the helicity of the exchanged photon, it measures the longitudinal/transverse production ratio $R=\sigma_L/\sigma_T$. Assuming SCHC and natural parity exchange, the predicted decay-muon angular distribution is[21]

$$W(\theta,\Delta\phi)=[3/16\pi(1+\varepsilon R)]\{1+\cos^2\theta+2\varepsilon R\sin^2\theta-\varepsilon\sin^2\theta\cos 2\Delta\phi+V(\theta,\Delta\phi)\}.$$

Here θ is the polar decay muon angle and $\Delta\phi$ is the azimuthal angle between the decay-muon plane and the lepton-scattering plane, as defined in the helicity frame by Schilling and Wolf[20]. The ratio ε of longitudinal to transverse photon flux[22] averages ≈ 0.8 in BFP data. The function $V(\theta,\Delta\phi)$ includes terms which average to zero over $-\pi<\Delta\phi<\pi$, when multiplied by unity or by $\cos 2\Delta\phi$. Neglecting this function, the curly bracket is proportional to $1-\alpha\cos 2\Delta\phi$, with

$$\alpha=\varepsilon\sin^2\theta/[1+\cos^2\theta+2\varepsilon R(Q^2)\sin^2\theta],$$

where the Q^2-dependence is displayed. BFP data with $Q^2<0.3$ (GeV/c)^2 are excluded to ensure adequate definition of the lepton scattering plane; data with $Q^2>5$ (GeV/c)^2 are excluded to prevent possibly large R at high Q^2 from making α too small to measure.

The objective of the BFP analysis is first to measure the azimuthal asymmetry coefficient α as a test of SCHC which is roughly independent of R. Secondly, the $\Delta\phi$-averaged polar-angle dependence $(1+\beta\cos^2\theta)$, with $\beta=[1-2\varepsilon R(Q^2)]/[1+2\varepsilon R(Q^2)]$, is used to measure R, i.e. the ψ helicity. This can reveal the photon helicity if SCHC in fact survives the first test. The statistical demands of this analysis are considerable. Figure 5 displays the ψ statistics (6693 events) from 75% of the BFP data. Final analysis of this sample is nearly complete. Available at present are preliminary results based on elastically produced ψ's corresponding to 20% of the data. Figure 6 shows the relative event rate vs. $\Delta\phi$, folded into one quadrant. Averaged over the range of the data in θ and Q^2, the fit coefficient α is 0.34 ± 0.12, very close to the SCHC expectation if $R=4Q^2/m_\psi^2$. Figure 7 exhibits the dependence of data averaged over $\Delta\phi$ upon $|\cos\theta|$, (a) for all data, and (b)-(d) divided into regions of increasing Q^2. The coefficient of $\cos\theta$ seems not to be invariant to the rise in Q^2. Rather, there is indication of a transition above $Q^2\approx 2$ (GeV/c)^2 from predominantly transverse to

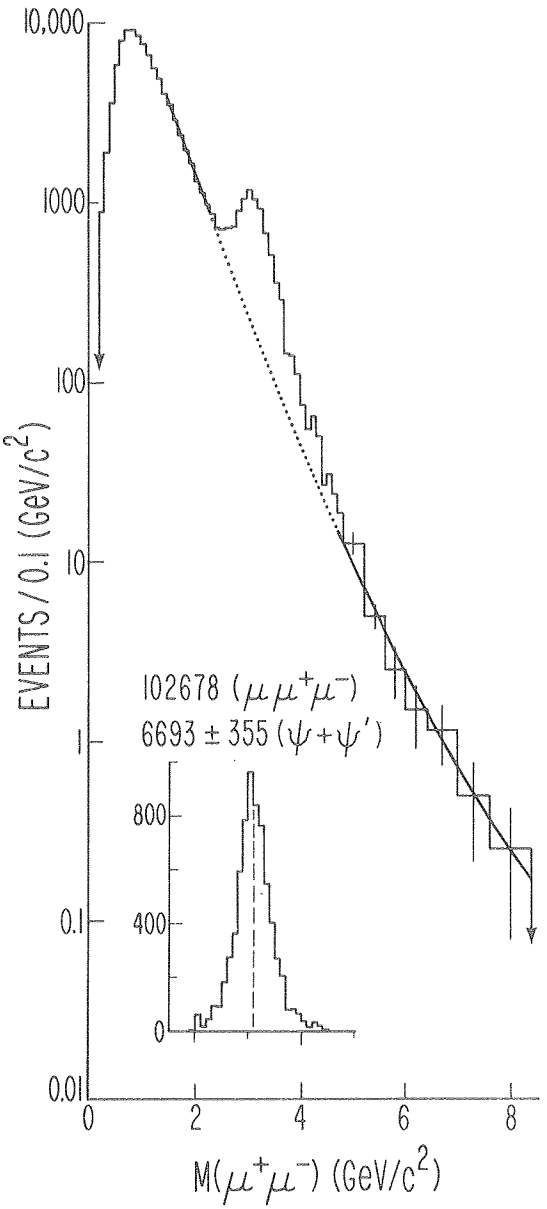

FIG. 5. Spectrum of 102 678 dimuon masses from 75% of BFP data, in the range $0<M(\mu^+\mu^-)<8.4$ $(GeV/c)^2$. The continuum is fit by $\exp(a+bM+cM^2)$ in the ranges indicated by the solid parts of the curve. The subtraction yields 6693±355 ψ's, with 9% mass resolution.

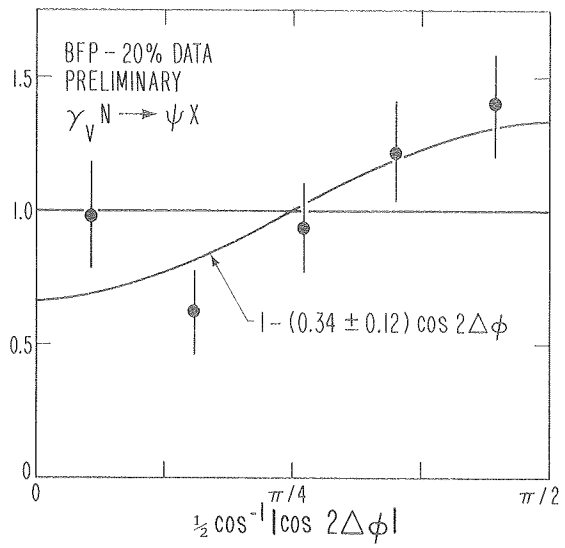

FIG. 6. Azimuthal distribution of elastically produced ψ's from preliminary BFP data, folded into one quadrant. The abscissa $\Delta\phi$ is the difference in azimuthal angle between the ψ-decay plane and lepton-scattering plane, defined in the helicity frame (Ref. 20). The best-fit curve is essentially the same as the SCHC prediction, if $\sigma_L/\sigma_T=4Q^2/m_\psi^2$.

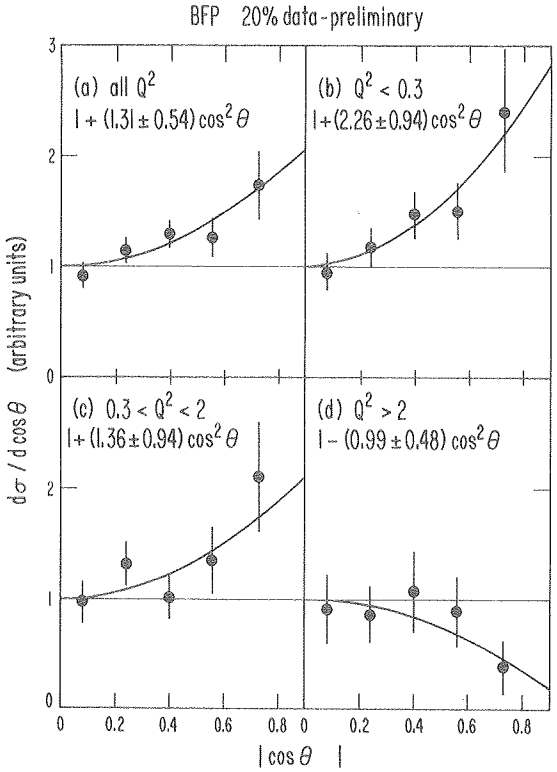

FIG. 7. Distribution in polar angle of decay muons from elastically produced ψ's, defined in the helicity frame (Ref. 20): (a) all BFP data; (b)-(d) data divided into three Q^2 regions. Best-fit curves and coefficients of $\cos^2\theta$ are shown.

predominantly longitudinal polarization. The fit to $R=\xi_\psi^2 Q^2/m_\psi^2$ yields $\xi_\psi^2=4.0^{+5.4}_{-2.1}$.

In summary, the preliminary BFP study of ψ polarization provides an internally consistent picture in which SCHC is valid and σ_L/σ_T rises rapidly with Q^2. The central value of the coefficient ξ_ψ^2 is almost one order of magnitude larger than the VMD extrapolation from lower-energy ρ and ϕ data[23], $\xi_{\rho,\phi}^2 \tilde{=} 0.5$. Since the relevant experiments all measure Q^2 up to $\approx m_V^2$, only in the ψ case is a major transverse→longitudinal transition apparent in the data. An inescapable corollary to this picture is that the measured ψ cross-section $\sigma_{eff}=(\sigma_T+\varepsilon\sigma_L)$ can possess a Q^2-dependence which is much flatter than that of σ_T. For example, if σ_{eff} is fit by $(1+Q^2/m_\psi{}^2)^{-2}$, and $\sigma_L/\sigma_T=4Q^2/m_\psi{}^2$, σ_T may be approximated by $(1+Q^2/\Lambda^2)^{-2}$ with $\Lambda\approx m_\psi/2$! Comparison of the Q^2-dependence of different data sets can likewise be difficult if the data arise from different θ regions. For example, the EMC ψ data are predominantly symmetric with θ near $\pi/2$, where the normalized longitudinal angular distribution $(3\sin^2\theta)/2$ is twice as prominent as the transverse distribution $3(1+\cos^2\theta)/4$. If feasible, in the future the Q^2-dependence of ψ-muoproduction data should conventionally be quoted near $\sin\theta=\sqrt{2/3}$, where the event rate is proportional to the full effective cross-section, independent of any Q^2-dependent shifts in the mix of longitudinal and transverse ψ polarization.

III. OPEN-CHARM MUOPRODUCTION

For the first time at this Rencontre, new results from BFP[6,7] and EMC extend substantially the published data[8] from the MSUF group on unbound $c\bar{c}$ production by muons. I shall first illustrate the case for charm interpretation of these data, using as an example the BFP analysis[6]. The resulting cross sections for charm production by muons and virtual photons will then be compared to existing data. Turning next to differential spectra, I shall review the comparisons between data and charm production models made by the three muon groups. After discussing EMC results on double charm decay, I will present the charm structure function extracted by the BFP analysis[7], and its contribution to inclusive scale-noninvariance.

A. Charm cross sections

All three muon experiments identify charmed states by their ≥3-body decays into muons. Particular charmed hadrons are unresolved. These states appear in the data samples in proportion to their production rate and leptonic branching ratio. Although not suited to first observation of charmed states, this continuum charm signature is the only reasonable explanation for most of the single-extra-muon final states observed in each experiment.

The BFP Multimuon Spectrometer[4,24], running conditions[4], and techniques of reconstruction[4] and charm analysis[6] are described elsewhere. Here I will

TABLE II. Mean values of reconstructed quantities for data before background subtraction, for charm MC, and for π,K-decay MC. The inelasticity is defined as 1-E(daughter μ)/ν. Errors are statistical.

Reconstructed kinematic quantity	Data	Monte Carlo Charm	Monte Carlo π,K→μ
<ν> (GeV)	127.0 ± 0.3	132.7 ± 0.3	109.8 ± 1.0
Geometric mean Q^2 $(GeV/c)^2$	0.767 ±.004	0.875 ±.006	0.562 ±.011
<Daughter μ energy> (GeV)	25.63 ±0.07	26.05 ±0.08	22.87 ±0.21
<Inelasticity>	0.785 ±.001	0.794 ±.001	0.773 ±.003
<Missing energy> (GeV)	14.03 ±0.14	13.60 ±0.18	2.25 ±0.53
<p(daughter)⊥ to γ_V> (GeV/c)	0.750 ±.003	0.677 ±.003	0.618 ±.008

TABLE III. Effects of fragmentation function $\mathcal{D}(z)$ on daughter energy and acceptance. To increase sensitivity to the choice of $\mathcal{D}(z)$, mean daughter energies are shown for γGF Monte Carlo with ν > 150 GeV.

$\mathcal{D}(z)$	<E(daughter μ)>	Relative acceptance
$(1-z)^{0.4}$	28.31 ± .15	1.00
$(1-z)^{3}$	26.94	0.81
$(1-z)^{-1.5}$ (z < 0.99)	29.78	1.20
Subtracted data	28.20 ± .20	

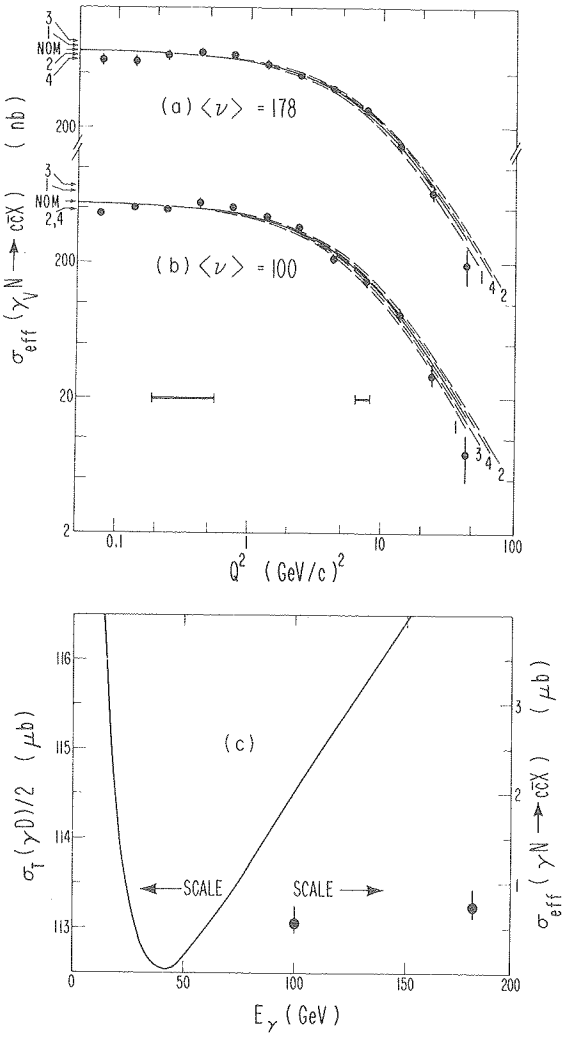

FIG. 8. Diffractive charm photoproduction cross sections from BFP data and the rise of the γN total cross section. Parts (a) and (b) show the extrapolation of the effective cross section to Q^2=0 at ν= (a) 178 and (b) 100 GeV. Errors are statistical. The solid curves are fits to $\sigma_0(1+Q^2/\Lambda^2)^{-2}$, with Λ= (a) 3.3 and (b) 2.9 GeV/c^2; the arrows labelled "NOM" exhibit σ_0. Systematic errors are parameterized by (1) decreasing, (2) increasing by 50% the subtracted π,K-decay background, and by recalculating the acceptance with a (3) softer, (4) harder quark fragmentation function as described in Table III. The effects on σ_0 are indicated by numbered arrows and the effects on Λ are indicated by dashed curves, normalized to the same σ_0. Part (c) compares σ_0 (data points, right scale) with a fit (Ref. 26) to half the total photon-deuteron cross section (curve, left scale).

call attention only to a few crucial aspects of the analysis. Table II compares mean values of experimental and Monte Carlo (MC) distributions. The charm MC is based on the γGF model using a c→D meson fragmentation function[25] $\mathcal{D}(z)=(1-z)^{0.4}$,

and assumes a yield of 0.187 decay muons per charmed quark pair. The π, K-decay MC is model-independent, using experimental data as input. The comparison in Table II rules out any possibility that π and K decay explain the data. Excluding data with $\nu<75$ GeV, the absolutely normalized π, K-decay rates account for (19±10)% of the BFP sample, where the error is systematic. Backgrounds from partially reconstructed muon tridents, and $\tau\bar{\tau}$ and b quark pairs are negligible[6]. Table III shows the effect on acceptance and mean daughter energy of varying the fragmentation function $\mathcal{D}(z)$ beyond the range favored both by these and by SPEAR data[25]. Quoted errors in BFP results include allowance for the $\mathcal{D}(z)$ and background variations.

Based on 20072 final states containing one extra muon, the BFP cross section for diffractive charm production at 209 GeV is $\sigma_{diff}(\mu N\to\mu c\bar{c}X)=6.9^{+1.9}_{-1.4}$ nb, 37% higher than the γGF prediction. "Diffractive production" refers to creation of $c\bar{c}$ pairs carrying most of the laboratory energy of the virtual photon, as in the γGF and VMD models. The BFP analysis is insensitive to other mechanisms producing charm nearly at rest in the γN center of mass. The effective photon cross section σ_{eff} is obtained from BFP data by factoring out the equivalent flux[22] of transversely polarized virtual photons. The extrapolation of σ_{eff} to $Q^2=0$ using a VMD propagator $(1+Q^2/\Lambda^2)^{-2}$ is shown in Fig. 8 (a,b). The best fits to Λ are 3.3±0.2 and 2.9±0.2 GeV/c^2 for $\nu=178$ and 100 GeV, and the $Q^2=0$ intercepts are 750^{+180}_{-130} and 560^{+200}_{-120} nb, respectively. The rise of 190^{+34}_{-52} nb in the charm photoproduction cross section is significant; the difference of 0.39±0.18 GeV/c^2 in Λ suggests some ν-dependence in the Q^2 shape. Except in the last case, the errors are largely systematic. The diffractive charm production rate is too small to saturate the rise[26] of the total γN cross section above 50 GeV (Fig. 8(c)). Using BFP results[4] corresponding to a 25±8 nb elastic ψ photoproduction cross section at 100 GeV, the BFP open-charm data fix the ratio of elastic ψ to diffractive charm production at 0.045±0.022, ∿2.5× the VMD prediction[9]. In that picture this result suggests that *non*-diffractive production is a significant fraction of the total charm-photoproduction cross section. Independent of VMD, BFP data and the analysis of Ref. 9 produce the limit $\sigma_{total}(\psi N)\geq 0.9$ mb (90% confidence).

The MSUF cross section for charm muoproduction at 275 GeV is 3±1 nb[8]. Corrected via γGF to 209 GeV, it is ∿1/3 of the BFP result. Acceptance limitations make interpretation of the MSUF data highly model-dependent. The EMC charm signal is described[2] as consistent in size with the γGF prediction, within cuts. The ≈600 nb cross section recently reported[27] for D^o photoproduction at 100 GeV is as large as the BFP extrapolation to $Q^2=0$ of *all* diffractive charm production. The photoproduction analyses[27] assumed an energy-independent cross section, unlike that found in the BFP data (Fig. 11(a); Fig. 12).

B. Differential charm-production spectra

Comparison of MSUF, EMC, and BFP data with models for $c\bar{c}$ production and single charm decay to muons is made in Figs. 9,10, & 11, respectively, and summarized in Table IV. Indicated in each figure is the calculated π, K-decay background, which is also subtracted from the BFP data. The MSUF data/model agreement is marginal, particularly for the inelasticity. Use of the γGF rather than the BN model[11] might improve the agreement. Within the EMC statistics (corresponding to $\sim$500 events as in the MSUF case), agreement is fairly good with a γGF model having parameter set "I" listed in Table IV. Parameter set "II" is a somewhat better fit. In either case, the experimental elasticity z is more steeply distributed than the model, with a tail suggesting contamination from partially reconstructed muon tridents. Within the BFP statistics (20072 events), agreement with the γGF model described earlier is acceptable in ν. The Q^2, E_{daughter}, and inelasticity distributions are similar in data and MC. The missing energy is different at the level of systematic uncertainty in calorimeter calibration, and the experimental daughter $p_\perp$ is high by 15%. The latter variable is sensitive to diffractive slope and charm decay parameters which are not part of

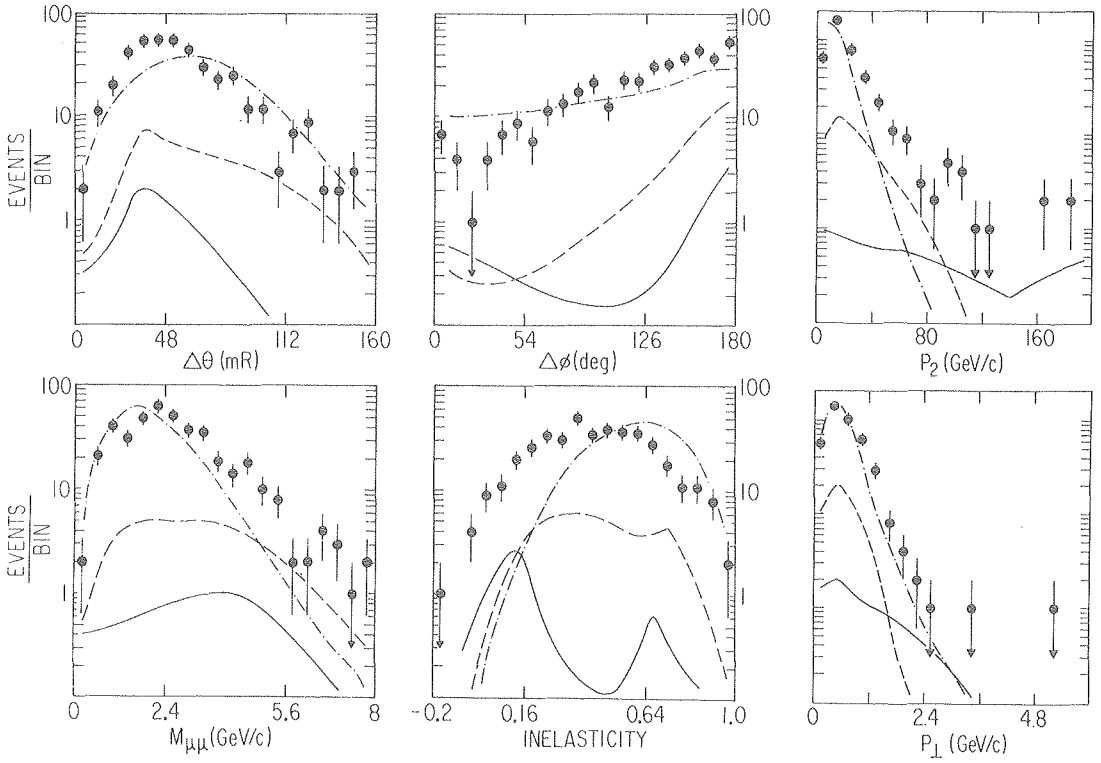

FIG. 9. Differential spectra of 412 MSUF single-charm-decay events in $\Delta\theta=\cos^{-1}(\hat{P}_1\cdot\hat{P}_2)$; $\Delta\phi$=difference in azimuth with respect to beam; P_2=produced μ momentum; $M_{\mu\mu}$=dimuon mass; [unconventional] inelasticity=$1-(E_1+E_2)/E_0$; and $P_\perp$= component of P_2 $\perp$ to the virtual photon. The upper (dash-dot), lower (dash), and solid curves are calculations for the charm model (Ref. 11); π,K and prompt μ background; and partially reconstructed μ tridents, respectively. Acceptance is not unfolded.

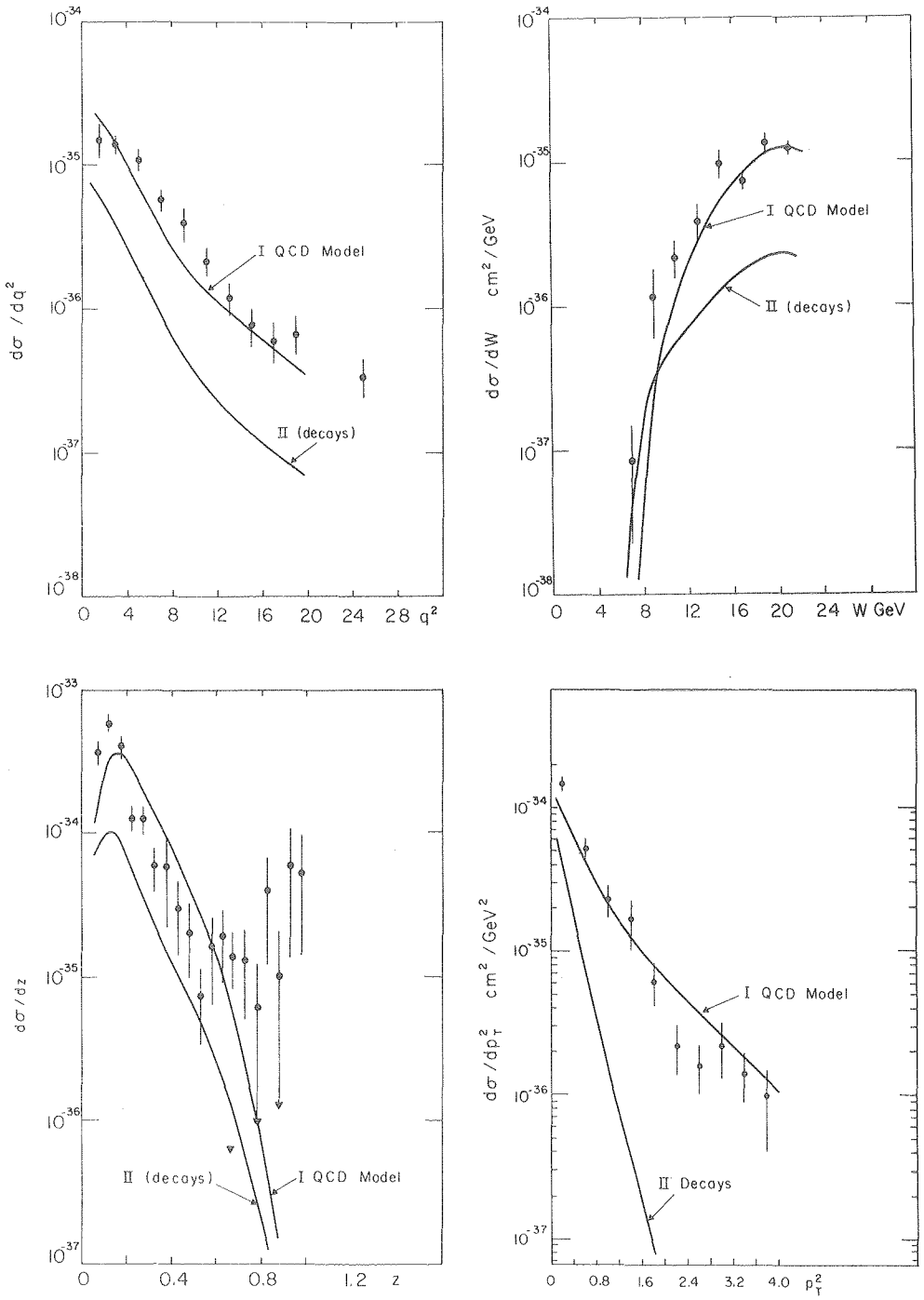

FIG. 10. Differential spectra of 497 EMC single-charm-decay events in q^2; $W=(2m_p\nu-q^2)^{\frac{1}{2}}$; z=produced E_μ/ν; $p_T{}^2$=square of produced μ momentum $\perp$ to the virtual photon. Geometrical acceptance is unfolded, except for the effects of the kinematic cuts $\nu/\nu_{max}<0.91$, $E_{\text{scattered }\mu}>20$ GeV, $\theta_{\text{scattered}}>0.007$, $E_{\text{produced }\mu}>16$ GeV, $Q^2>1$ (GeV/c)^2. Curves (I) are a photon-gluon-fusion charm calculation using parameters (I) in Table IV. Curves (II) are calculated π,K-decay background.

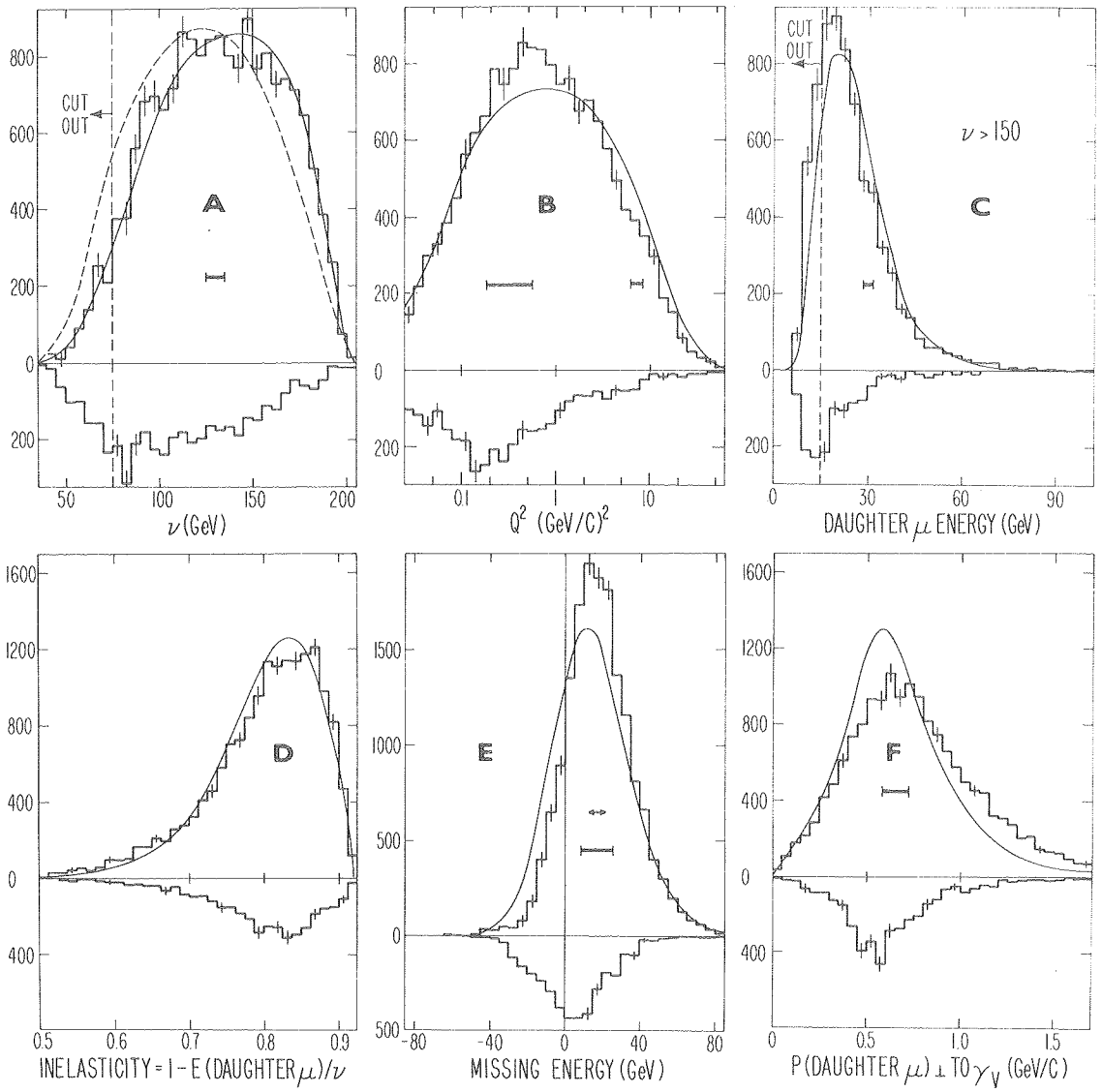

FIG. 11. Differential spectra of 20 072 BFP single-charm-decay events in (a) energy transfer, (b) momentum transfer-squared, (c) daughter muon energy, (d) inelasticity, (e) missing (neutrino) energy, (f) daughter muon $p_\perp$. The ordinates are events per bin with acceptance not unfolded. Inverted histograms show the simulated π,K-decay background, normalized to the beam flux. Erect histograms exhibit background-subtracted data. Errors are statistical. The curves, normalized to these data, are the photon-gluon-fusion charm calculation. The dashed curve in (a) represents an alternate model (Ref. 27) in which $D\bar{D}$ pairs are produced with ν-independent probability. Events in (c) have ν>150 GeV. Horizontal brackets exhibit typical rms resolution. The arrow in (e) shows the shift caused by a ±2.5% excursion in calorimeter calibration.

the γGF model. Overall, in a first confrontation with the data, photon-gluon fusion has succeeded beyond expectation. Additional model comparison using the ν-dependence of σ_{eff} is provided by BFP data in Fig. 12. Despite the agreement with the $3(1-x)^5/x$ gluon distribution, systematic uncertainties prevent the analysis from ruling out the BN model, or two alternative choices for the gluon x distribution. The data do reject the assumption[27] that σ_{eff} is ν-independent.

TABLE IV. Comparison of results on muoproduction of charmed states decaying to muons.

	MSU-FNAL (Ref. 8)	EMC	BFP (Ref. 6 , 7)
Events: 1 decay μ	412	497	20072
2 decay μ's	-	120	-
π,K-decay background to 1-decay-μ events	15%	~20% (→ 10% after $p_\perp$ cut)	19%
Charm model used	Bletzacker and Nieh (Ref. 11)--phenomenological "photon dissociation"	Photon-gluon fusion $xG(x)=a(1-x)^b$ $\mathcal{D}(z)=(1-z)^c$	
Model parameters used		I. a=3, b=5, c=-∞, Λ=0.5, m_c=1.86 II. a=1.9, b=4, $\mathcal{D}(z)$=exp(2.3z), Λ=0.35, m_c=1.5	I. a=3, b=5, c=0.4, Λ=0.5, m_c=1.5 II. c=3 III. c=-1.5 (z<0.99)
Problems in model comparisons	Inelasticity in poor agreement	3μ feed-down and other disagreement in elasticity plot	p(produced μ) ⊥ to γ_V is 15% higher in data
σ(μN→μcc̄X) "diffractive"	3±1 nb (E_0=275) =>~2 nb (E_0=209)	Consistent with photon-gluon fusion within cuts	$6.9^{+1.9}_{-1.4}$ nb (E_0=209) 1.37× photon-gluon fusion

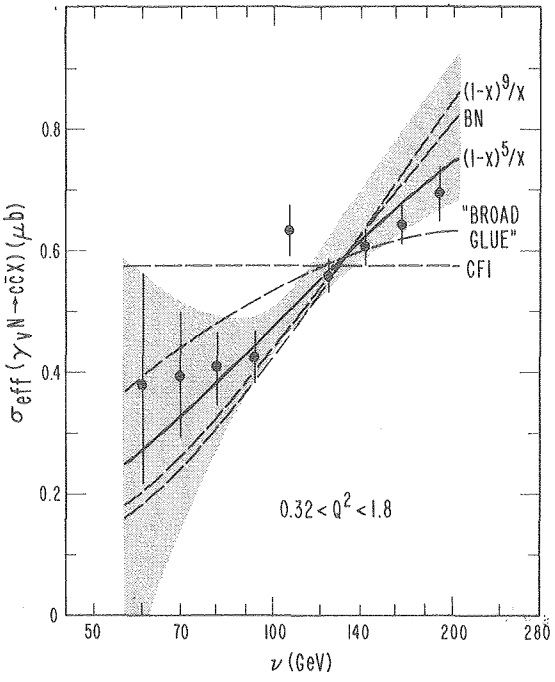

FIG. 12. Energy-dependence of the effective cross section σ_{eff} for diffractive charm photoproduction in BFP data. For $0.32<Q^2<1.8(\mathrm{GeV/c})^2$, σ_{eff} varies with Q^2 by ≲20%. Errors are statistical. The solid curve exhibits the ν-dependence of the photon-gluon-fusion model with parameters (I) in Table IV and represents the data with 13% confidence. Other gluon-distribution choices $(1-x)^9/x$, and "broad glue" $(1-x)^5(13.5+1.07/x)$ are indicated by dashed curves. The dashed curve labelled BN is the phenomenological parameterization of Ref. 11, and the dashed line labelled CFI represents the energy-independence assumed by recent photoproduction analyses (Ref. 27). Curves are normalized to the data. The shaded band exhibits the range of changes in shape allowed by systematic error. For clarity it is drawn relative to the solid curve. Data below ν=75 GeV are cut out.

C. Double charm decay to muons

An ambitious program to identify $c\bar{c}$ production in which both charmed states decay to muons has been undertaken by EMC[2]. The analysis favors events with hadronic showers relative to those with electromagnetic showers in the calorimeter by exploiting the longitudinal energy-deposit profile. After cuts on dimuon mass ($1<M_{\mu\mu}<2.5$ GeV/c^2) and elasticity ($z<0.6$), a significant ($\approx$44 GeV) average missing energy is observed in the 20 events having a reconstructed scattered muon. This is evidence for two decay neutrinos in the final state. Distributions similar to those in Fig. 10 are exhibited for 120 double-charm-decay candidates in Fig. 13. Absolute agreement of these distributions with the γGF calculation is an important preliminary result. It indicates that the momentum fractions of the quark and antiquark in the charmed sea are positively correlated, as predicted by photon-gluon fusion; otherwise, one of the charmed states would almost always be produced too slow to yield an observable decay muon. Similar data can be expected ultimately to quantify that correlation, subjecting γGF to a clean test.

D. The charm structure function and its contribution to scale-noninvariance

The BFP analysis[7] defines the charm structure function $F_2(c\bar{c})$ through the relation

$$Q^4\nu d^2\sigma(c\bar{c})/dQ^2d\nu=4\pi\alpha^2(1-y+y^2/2)F_2(c\bar{c}).$$

Here y is ν/ν_{max} and $\sigma(c\bar{c})$ is the cross section for diffractive charm muoproduction. $F_2(c\bar{c})$ plays the same role in charm production as would F_2 in inclusive scattering if absorption of longitudinally polarized photons were negligible; in the same approximation it is $4x_B c(x_B)/9$, where $c(x_B)$ is the charmed-sea distribution.

Figure 14 exhibits the Q^2-dependence of $F_2(c\bar{c})$ obtained by BFP for two values of fixed average ν. At its peak $F_2(c\bar{c})$ is $\sim$4% of F_2. None of the models fully represents the data. The γGF shapes for m_c=1.5 and 1.2 GeV/c^2 are nearly degenerate, since they depend on $m_{c\bar{c}}$, which cannot be less than $2m_D$[12]. The maxima predicted by both the γGF and BN models resemble the data in shape and in ν-dependence, but occur at higher Q^2. The ψ-dominance functions drop too slowly at high Q^2. Systematic errors are only weakly correlated with Q^2 and do not obscure the disagreement.

In the energy range of the data in Fig. 15, $F_2(c\bar{c})$ is clearly scale-noninvariant for $Q^2<10$ (GeV/c)^2, or $x_B\lesssim 0.07$. To model the charm contribution to F_2 for smaller photon energies, the γGF model is normalized to the data and damped at high Q^2 by the factor $(1+Q^2/(10\text{ GeV/c})^2)^{-2}$. The resulting family of dashed curves in Fig. 15 adequately matches the BFP data.

A full description of the effect of charm production on F_2 must include the

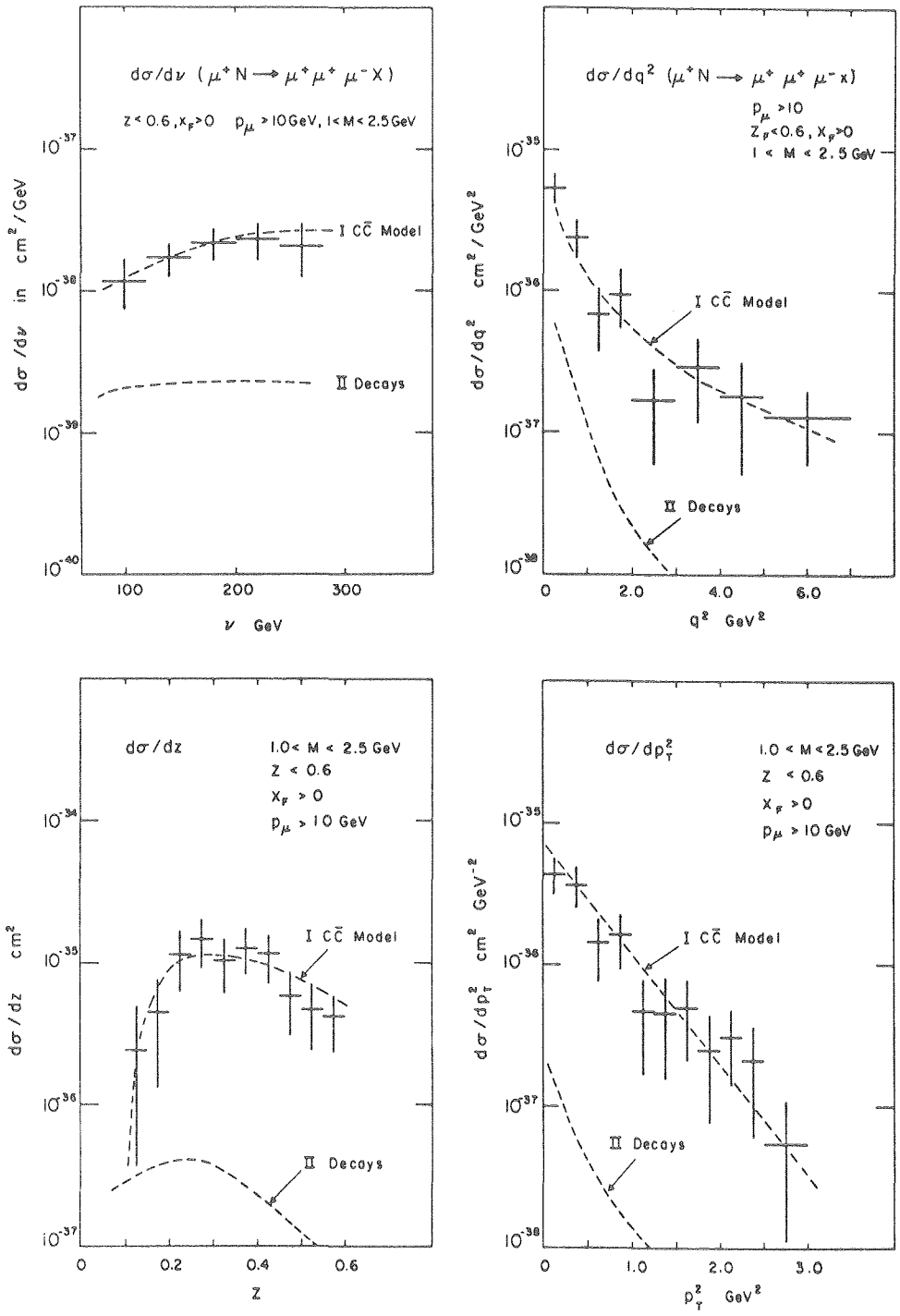

FIG. 13. Differential spectra of 120 EMC double-charm-decay events in ν; q^2; z=produced μ pair energy/ν; and p_T^2=produced μ pair momentum $\perp$ to the virtual photon. Geometrical acceptance is unfolded, except for the effects of the indicated cuts. Curves (I) and (II) are as in Fig. 10.

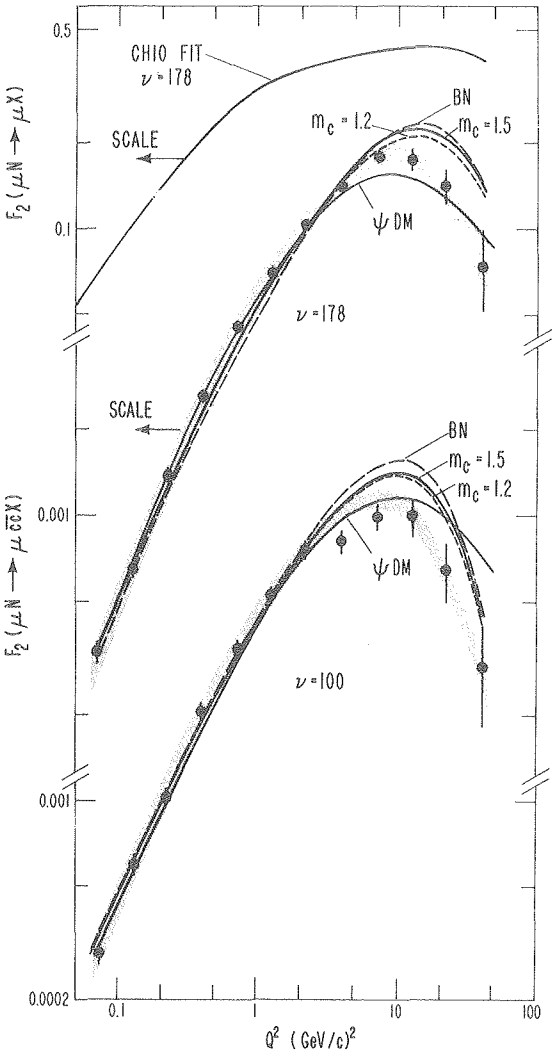

FIG. 14. Q^2-dependence of the structure function $F_2(c\bar{c})$ for diffractive charm muoproduction in BFP data. At each of two average photon energies, each curve is normalized to the data. Errors are statistical. The solid (short dashed) curves labelled m_c=1.5 (1.2) exhibit the photon-gluon-fusion prediction with a charmed quark mass of 1.5 (1.2) GeV/c^2. Solid curves labelled ψDM correspond to a ψ-dominance propagator, and long-dashed curves labelled BN are the model of Ref. 11. Shown at the top is a fit adapted from Ref. 28 to the inclusive structure function F_2 for isospin-0 μN scattering. The shape variations allowed by systematic errors are represented by the shaded bands.

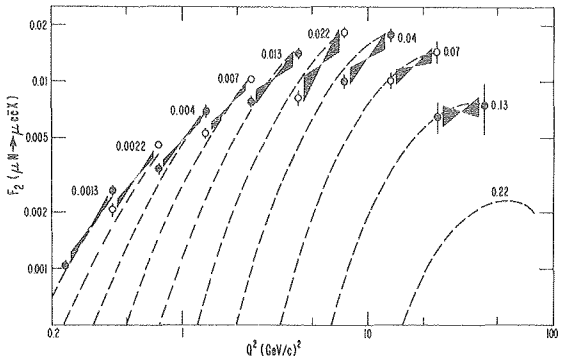

FIG. 15. Scale-noninvariance of $F_2(c\bar{c})$. BFP data points are arranged in pairs, alternately closed and open. The points in each pair are connected by a solid band and labelled by their common average value of $x_B=Q^2/2m_p\nu$. Errors are statistical. The dashed lines are the prediction of the photon-gluon-fusion model with m_c=1.5 GeV/c^2 except that the model is renormalized and damped at high Q^2 as described in the text. The solid bands represent the slope variations allowed by systematic errors.

charmonium contribution. The ψ-muoproduction rate[4] agrees with the unmodified γGF prediction if elastic ψ production accounts for 1/6 of all charmonium production[14]. Adopting this model, BFP augments the measured[6] $6.9^{+1.9}_{-1.4}$ nb open charm cross section by 2.8 nb of bound charm production. This increases the maximum charm contribution to inclusive scale-noninvariance only by ∿15%. Table V compares fit[28] inclusive $\partial F_2/\partial \ell n Q^2$ at fixed x_B to $\partial F_2(c\bar{c})/\partial \ell n Q^2$ augmented for charmonium production, calculated with the (γGF) model that has been matched to the muoproduction data. Where charm scale-noninvariance is most important, the calculation is reliable to ∿±40%.

TABLE V. Calculated $10^4 \partial F_2/\partial \ell n Q^2$ at fixed x_B vs. ν (top), Q^2 (left margin), and x_B (diagonals, right margin). For each Q^2-ν combination, two values are shown. The bottom value is fit to the structure function F_2 for μN scattering (Ref. 28). The top value is the contribution $F_2(c\bar{c})$ to F_2 from diffractive muoproduction of bound and unbound charmed quarks, calculated by BFP using a model matched to their data.

ν(GeV)	27	42	67	106	168	
Q^2 (GeV/c)^2	$\frac{10^4 \partial F_2(c\bar{c})/\partial \ell n Q^2}{10^4 \partial F_2(\mu N)/\partial \ell n Q^2}$					x_B
0.63	17 / 1070	30 / 1090	43 / 1110	54 / 1120	58 / 1130	
1.0	23 / 980	43 / 1010	63 / 1040	77 / 1050	84 / 1060	0.002
1.6	30 / 650	59 / 680	87 / 700	107 / 720	116 / 730	0.003
2.5	36 / 310	73 / 340	110 / 350	139 / 360	146 / 360	0.005
4.0	36 / 320	80 / 390	128 / 430	162 / 460	163 / 480	0.008
6.3	29 / 210	75 / 330	128 / 410	165 / 460	154 / 490	0.013
10	15 / 50	54 / 220	104 / 340	138 / 430	112 / 480	0.020
16	4 / -130	27 / 50	64 / 230	90 / 360	52 / 440	0.032
25	-2 / -189	7 / -126	26 / 50	40 / 230	0 / 370	0.050
40	0 / -31	-1 / -171	6 / -122	10 / 50	-22 / 240	0.080
63		0 / -23	1 / -154	1 / -119	-16 / 50	0.130

The conclusion is that diffractive charm production is responsible for ∿1/3 of the total inclusive scale-noninvariance in a region bounded by $2<Q^2<13(\mathrm{GeV/c})^2$ and $50<\nu<200$ GeV, and centered at $x_B \approx 0.025$. This region provided most of the original evidence[29] for scale-noninvariance in muon scattering. VMD arguments[9] raise the possibility that non-diffractive charm muoproduction might add substantially to the diffractive scale-noninvariance measured by BFP. Deeper implications of scale-noninvariance in muon scattering can be understood only by first correcting for such effects, which depend on charmed-quark-pair masses and therefore have a kinematic origin.

I appreciate the many contributions of my colleagues in the Berkeley-Fermilab-Princeton group to the work I have reviewed. In particular, it is a pleasure to acknowledge the collaboration of G.D. Gollin in preparing the BFP open-charm results. Members of the EMC, MSUF, and BCDMS muon experiments have most generously discussed their data. It is a privilege to have attended so well-organized a conference.

The author is supported by the High Energy Physics Division of the U.S. Department of Energy under Contract No. W-7405-Eng-48.

REFERENCES

1) A.R. Clark, K.J. Johnson, L.T. Kerth, S.C. Loken, T.W. Markiewicz, P.D. Meyers, W.H. Smith, M. Strovink, W.A. Wenzel (Berkeley); R.P. Johnson, C. Moore, M. Mugge, R.E. Shafer (Fermilab); and G.D. Gollin, F.C. Shoemaker, and P. Surko (Princeton).
2) CERN-DESY (Hamburg)-Freiburg-Kiel-Lancaster-LAPP (Annecy)-Liverpool-Oxford-Rutherford-Sheffield-Turin-Wuppertal collaboration. The author is grateful to C. Best, F. Brasse, J. Davies, E. Gabathuler, and T. Sloan of this group for discussions on the EMC data, which are also described in J. Davies' report to this Rencontre.
3) A. Benvenuti, in Proc. Int. Symp. on Lepton and Photon Interactions at High Energies (Fermilab, Batavia, Ill., 1979).
4) A.R. Clark et al., Phys. Rev. Lett. 43, 187 (1979).
5) J.J. Aubert et al., Phys. Lett. 89B, 267 (1980).
6) A.R. Clark et al., LBL-10747, submitted for publication.
7) A.R. Clark et al., LBL-10879, submitted for publication.
8) D. Bauer et al., Phys. Rev. Lett. 43, 1551 (1979), and references cited therein.
9) D. Sivers, J. Townsend, and G. West, Phys. Rev. D13, 1234 (1976).
10) See e.g. S. Okubo, Phys. Lett. 5, 160 (1963).
11) F. Bletzacker and H.T. Nieh, SUNY-Stony Brook Report No. ITP-SB-77-44 (unpublished).
12) J.P. Leveille and T. Weiler, Nucl. Phys. B147, 147 (1979), and references cited therein.
13) S. Brodsky and G. Farrar, Phys. Rev. Lett. 31, 1153 (1973).
14) V. Barger, W.Y. Keung, R.J.N. Phillips, Univ. of Wisconsin Report No. 79-0776 (unpublished).
15) K. Berkelman, summary of DORIS results presented to this Rencontre.
16) M. Glück and E. Reya, Phys. Lett. 79B, 453 (1978).
17) T. Weiler, Phys. Rev. Lett. 44, 304 (1980).
18) U. Camerini et al., Phys. Rev. Lett. 35, 483 (1975).
19) J.P. Leveille and T. Weiler, Phys. Lett. 86B, 377 (1979).
20) K. Schilling and G. Wolf, Nucl. Phys. B61, 381 (1973).
21) T.W. Markiewicz, Ph.D. Thesis, University of California, Berkeley, 1980 (in preparation).
22) F.J. Gilman, Phys. Rev. 167, 1365 (1968).
23) J.T. Dakin et al., Phys. Rev. Lett. 30, 142 (1973); W.R. Francis et al., Phys. Rev. Lett. 38, 633 (1977); R. Dixon et al., Phys. Rev. Lett. 39, 516 (1977).
24) G. Gollin et al., IEEE Trans. Nuc. Sci. NS-26, 59 (1979).
25) P.A. Rapidis et al., Phys. Lett. 84B, 507 (1979).
26) D.O. Caldwell et al., Phys. Rev. Lett. 42, 553 (1979).
27) M.S. Atiya et al., Phys. Rev. Lett. 43, 414 (1979); P. Avery et al., Univ. of Illinois Report No. UI-HEPG-1980-1 (to be published).
28) B.A. Gordon et al., Phys. Rev. D20, 2645 (1979).
29) Y. Watanabe et al., Phys. Rev. Lett. 35, 898(1975); C. Chang et al., Phys. Rev. Lett. 35, 901 (1975).